Scientia Iranica, Vol. 14, No. 3, pp 251–262

SCIENTIA IRANICA

Development and Application of Compressible Vorticity Confinement

M. Malek Jafarian[1] and M. Pasandideh Fard*

In this paper, variable confinement parameters were successfully developed for compressible vorticity confinement. Three variable confinement parameters, that have velocity dimension, were defined, based on three artificial dissipation schemes. The resulting confinement parameters are functions of the spectral radii of the Jacobian matrices and the Jacobian matrices themselves. Therefore, the confinement parameter implicitly contains the grid size and other local fluid properties. Preliminary results for moving vortices showed that the new confinement parameters allow the capture of vortical layers that, effectively, do not decay in time, like Hu et al.'s confinement. Calculations of the supersonic base flow and supersonic shear layer showed good agreement with experimental and analytical data, especially for the variable CUSP confinement parameter. When variable confinement parameters are used, the tuning constant is equal to, or larger than, the equivalent value of the constant confinement (Hu et al.). This means that the tuning constant varies in a range smaller than that of the Hu et al. constant confinement, especially for the CUSP confinement parameter.

INTRODUCTION

Many flows of interest are characterized by large regions of concentrated vortical structures that persist and can convect over long distances. Flows of this nature include those associated with aircraft, in particular, rotorcraft, ships, automobiles, bridges and buildings. Conventional CFD methods tend to dissipate vortical structures, degrading the overall accuracy of the computed flows. This dissipation can be reduced through the use of fine grids, but, at the expense of greatly increased computational demands. For example, flow computations around 3D complex bodies with large-scale separations and vortices are difficult within the realistic number of grid points. A natural way to tackle such kinds of problem is by using high-order schemes and/or automatic grid refinement techniques, in order to increase the accuracy of the resolution and, thus, avoiding a too fast dissipation of the vortical structures [1-3]. Higher order discretization increases CPU loading and adaptive procedures have a lot of complex logic controls.

1. *Department of Mechanical Engineering, Ferdowsi University, P.O. Box 91775-1111, Mashhad, I.R. Iran.*

*. *Corresponding Author, Department of Mechanical Engineering, Ferdowsi University, P.O. Box 91775-1111, Mashhad, I.R. Iran.*

Another method is to use Direct Numerical Simulation (DNS) or Large Eddy Simulation (LES), by which, the complete time-dependent Navier-Stokes equations are solved. Although these methods are very accurate, with no significant numerical errors, they are computationally exhaustive, especially for complex 3D flows. As a result, DNS or LES are still not considered practical CFD methods [4].

Therefore, the vorticity confinement method has been proposed to reduce the diffusive property of the incompressible vortical flow simulations by Steinhoff and co-workers [5-7]. In this method, the source term added to the Navier-Stokes equations works as it convects the discretization error back into the vortex center and, thus, confines the vortex. The confinement adds acceleration in a direction that is normal to the vorticity and to the gradient of vorticity vectors. This has the effect of adding a velocity correction that convects vorticity in the opposite direction to the numerical diffusion [8] (for further discussion see [7]). Such methodology has been successfully applied to very different types of flowfield, from simple vortices to complex rotor-fuselage interactions. This is done using an extension of the method to general body surfaces with simple Cartesian grids [9-11] and even to massively separated flows.

There have been several attempts by Pevchin [12] and Yee and Lee [13] to extend the vorticity con-

finement to compressible flows. But, the method has been generalized to compressible flows by Hu et al. [8] considering the corresponding source term as a body force, for which a complementary term must consistently be added to the energy equation, due to the work done by this body force term. Hu et al. [8] have worked mainly on uniform Cartesian grids, for which the confinement parameter could be kept constant. However, in spite of the success of the method with regard to its goals, the confinement term is proportional to an empirical parameter, such as artificial viscosity for shock capturing, and the influence of this parameter on the solution is also questionable.

Murayama [14] attempted to use this type of vorticity confinement on an unstructured grid, leaving the confinement parameter constant. The results were mixed. For some values of the confinement parameter, an improvement of results was observed. Other values of the confinement parameter lead to unrealistic predictions. These results make it clear that, for non-uniform grids, a general solution has to be found. Fedkiw et al. [15] used vorticity confinement for the visual simulation of smoke on Cartesian grids, using incompressible Navier-Stokes equations. They used an explicit, linear dependence on the mesh size for the confinement parameter. Lohner and Yang [16] used a general incompressible vorticity confinement term that has been derived using a dimensional analysis for unstructured grids. The resulting vorticity confinement is a function of the local vorticity-based Reynolds number, the local element size, the vorticity and the gradient of the absolute value of the vorticity. Also, Costes and Kowani [17] implemented an automatic vorticity confinement procedure, in order to conserve vorticity in the resolution of the compressible Euler equations. It is based on the cancellation of the leading truncation error terms in the numerical solution of the vorticity convection equation. The results obtained so far indicate that this way of research is promising. However, it is shown that, for fine grids, a regularization treatment must also be applied at the center of the vortex, because of the vorticity confinement singularity.

As pointed out in [16], a dimensional analysis of the confinement term shows that confinement parameter (E_c) has the dimension of a velocity. This means that, for a given grid and configuration, a proper choice of this parameter should be dependent on the free stream conditions of the incoming flow-field. Furthermore, any automatic tuning of this parameter must conserve the same dimensions [17].

Consequently, the objective of this paper is the development and application of the compressible vorticity confinement method in 2-D flows. New and general formulations have been proposed for the compressible confinement parameter, which have the velocity dimension. The three new confinement parameters are: Functions of the spectral radii of the flux Jacobian matrix (derived from the SCalar Dissipation Scheme), the Jacobian matrix itself (derived from the MAtrix Dissipation Scheme) and features of the CUSP (Convective Upstream Split Pressure) dissipation scheme.

These are applied for convecting an isolated 2-D vortex inside uniform and non-uniform Cartesian meshes, also, a supersonic base flow and supersonic shear layer. The results are compared with the Hu et al. experimental and analytical data to show the performance of the authors contributions.

GOVERNING EQUATIONS AND COMPRESSIBLE VORTICITY CONFINEMENT (CVC) FORMULATION

There have been several attempts to extend the vorticity confinement to compressible flows. The main issue is concerning how to add the confinement term in a consistent manner within a conservation law framework. Pevchin et al. [12] developed a complicated formulation, based on flux splitting that was dependent on grid orientation. Yee and Lee [13] attempted to utilize the incompressible confinement term into the compressible momentum equations. Finally, Hu et al. [8] noticed that the confinement may be considered to be a body force that can be added to the integral momentum equation and the rate of work done by the body force added to the energy conservation law. Considering the Euler equations in the Cartesian coordinate:

$$Q_t + f_x + g_y = S, \tag{1}$$

where:

$$Q = \begin{bmatrix} \rho \\ \rho u \\ \rho \nu \\ e \end{bmatrix}, \qquad f = \begin{bmatrix} \rho u \\ \rho u^2 + P \\ \rho u \nu \\ u(e+P) \end{bmatrix},$$

$$g = \begin{bmatrix} \rho v \\ \rho u \nu \\ \rho \nu^2 + P \\ \nu(e+P) \end{bmatrix}, \qquad S = \begin{bmatrix} 0 \\ \rho \vec{f}_b.\hat{i} \\ \rho \vec{f}_b.\hat{j} \\ \rho \vec{f}_b.\hat{V} \end{bmatrix},$$

Q is the vector of conserved variables, f and g are the flux vectors and S is the vorticity confinement vector. The independent variables are time (t) and Cartesian coordinates (x, y). ρ, u, v, e and P denote non-dimensional density, Cartesian velocity components, energy and pressure, respectively. $\vec{f}_b$ is a body force per unit mass, which serves to try to balance the numerical diffusion inherently related to numerical discretization and to conserve momentum in vortical regions:

$$\vec{f}_b = \quad E_c \hat{n}_c \times \vec{\omega},$$

where:

$$\hat{n}_c = \frac{\nabla|\vec{\omega}|}{|\nabla|\vec{\omega}||} = \phi_{xs}\hat{i} + \phi_{ys}\hat{j},$$

$$\vec{\omega} = \vec{\nabla} \times \vec{Q},$$

E_c is the confinement parameter with the dimension of velocity. Hu et al. [8] showed that this parameter ranges from O(0.001) to O(0.1). Finally, the vorticity confinement term in a compressible flow can be expressed, as follows:

$$S = \begin{bmatrix} 0 \\ \rho E_c \omega_z \phi_{ys} \\ \rho E_c \omega_z \phi_{xs} \\ \rho E_c [u(\ \omega_z \phi_{ys}) + \nu(\omega_z \phi_{xs})] \end{bmatrix}. \quad (2)$$

If Equation 1 is transformed to arbitrary curvilinear coordinates, then, one obtains:

$$\hat{Q}_t + \hat{F}_\xi + \hat{G}_\eta = S, \quad (3)$$

where:

$$\hat{Q} = J^{-1} \begin{bmatrix} \rho \\ \rho u \\ \rho \nu \\ e \end{bmatrix}, \qquad \hat{F} = J^{-1} \begin{bmatrix} \rho U \\ \rho u U + \xi_x P \\ \rho \nu U + \xi_y P \\ (e+P)U \end{bmatrix},$$

$$\hat{G} = J^{-1} \begin{bmatrix} \rho V \\ \rho u V + \eta_x P \\ \rho \nu V + \eta_y P \\ (e+P)V \end{bmatrix},$$

and:

$$U = \xi_x u + \xi_y v, \qquad V = \eta_x u + \eta_y v,$$

where U and V are contravariant velocities written without metric normalization and J^{-1} is the inverse transformation Jacobian. Then, one obtains:

$$(J^{-1}Q)_t + F_\xi + G_\eta = S, \quad (4)$$

with:

$$F = f y_\eta - g x_\eta, \qquad G = g x_\xi - f y_\xi.$$

In a cell-centered finite volume method, Equation 4 is integrated over an elemental volume in the discretized computational domain and J^{-1} is identified as the volume of the cell. Equation 4, assuming J^{-1} to be independent of time, can be written, as follows:

$$J^{-1}Q_t + AQ_\xi + BQ_\eta = S, \quad (5)$$

where A and B are the flux Jacobian matrices defined by:

$$A = \frac{\partial F}{\partial Q}, \qquad B = \frac{\partial G}{\partial Q},$$

and the details of A and B matrices are presented in [18].

NUMERICAL FORMULATION

To advance the solution in time, the multi-stage scheme is applied. A typical step of a Runge-Kutta (5-stages) approximation to Equation 5 is:

$$Q^{(k)} = Q^{(0)} - \alpha_k \frac{\Delta t}{J^{-1}} [D_\xi F^{(k-1)} + D_\eta G^{(k-1)} - S - AD], \quad (6)$$

where:

$$\alpha_k = \left(\frac{1}{4}, \frac{1}{6}, \frac{3}{8}, \frac{1}{2}, 1\right), \quad (7)$$

D_ξ and D_η are spatial differencing operators and AD is the artificial dissipation term. Three artificial dissipation models have been used in this work, which will be presented in the next section. The bracketed superscript in Equation 6 refers to the stages of the Runge-Kutta scheme. In addition, local time stepping and implicit residual averaging are utilized to accelerate convergence.

ARTIFICIAL DISSIPATION SCHEMES

The artificial dissipation models have been developed to remove the spurious oscillations for the robustness of stability and the fast convergence of solutions in the steady-state aerodynamic sense. A combination of second and fourth differences of the flow variables is used to form the dissipation operator, AD. The second difference terms are used to prevent oscillations at shock waves, while the fourth difference terms are important for stability and convergence toward the steady state solution.

SCalar Dissipation Scheme (SCDS)

The basic elements of the SCDS model considered in this paper were first introduced by Jameson, Schmidt and Turkel [19] in conjunction with Runge-Kutta explicit schemes. This dissipation model has been used by many investigators [20] to solve, numerically, the Euler and Navier-Stokes equations for a wide range of fluid dynamic applications. In this section, the basic model is briefly reviewed.

Consider the dissipation model added to the right-hand side of Equation 6, where the dissipation model is divided into two terms in the ξ and η directions. The two SCDS terms are written as:

$$AD = \hat{D}_\xi + \hat{D}_\eta, \quad (8)$$

where $\hat{D}_\xi$ and $\hat{D}_\eta$ are the dissipation terms in the ξ and η directions, respectively. The SCDS term in the ξ direction is defined as:

$$\hat{D}_\xi = \frac{\left(\hat{d}_{i+\frac{1}{2},j} - \hat{d}_{i-\frac{1}{2},j}\right)}{\Delta\xi}, \quad (9)$$

where the numerical dissipation flux is:

$$\hat{d}_{i+\frac{1}{2},j} = |\lambda|_{i+\frac{1}{2},j}\left[\varepsilon^{(2)}_{i+\frac{1}{2},j}(Q_{i+1,j} \quad Q_{i,j}) \right.$$
$$\left. \varepsilon^{(4)}_{i+\frac{1}{2},j}(Q_{i+2,j} \quad 3Q_{i+1,j}+3Q_{i,j} \quad Q_{i \quad 1,j})\right], \tag{10}$$

where $|\lambda|$ is proportional to the largest eigenvalue of the Jacobian matrix, which is called the spectral radii of the Jacobian matrix. The absolute eigenvalue and transformation Jacobian in the generalized coordinates are, as follows:

$$|\lambda|_{i+\frac{1}{2},j} = \frac{1}{2}(|\lambda|_{i+1,j} + |\lambda|_{i,j}),$$

where:

$$|\lambda|_{i,j} = |q + c\sqrt{a_1^2 + a_2^2}|, \tag{11}$$

and:

$$a_1 = J \quad {}^1\xi_x, \qquad a_2 = J \quad {}^1\xi_y, \qquad q = a_1 u + a_2 v, \tag{12}$$

and c is the speed of sound. The nonlinear dissipation functions, $\varepsilon^{(2)}_{i+\frac{1}{2},j}$ and $\varepsilon^{(4)}_{i+\frac{1}{2},j}$, in Equation 10 determine the magnitudes of the second and fourth order dissipation terms, based on the change of the density gradient. The nonlinear dissipation functions depend on flow and are defined by Jameson et al. [19]. This model has an excellent shock capturing property and gives sufficient numerical stability to the central difference schemes.

MAtrix Dissipation Scheme (MADS)

In the standard MADS model of Swanson and Turkel [21], the artificial dissipation flux is given by:

$$\hat{d}_{i+\frac{1}{2},j} = |A|_{i+\frac{1}{2},j}\left[\varepsilon^{(2)}_{i+\frac{1}{2},j}(Q_{i+1,j} \quad Q_{i,j}) \right.$$
$$\left. \varepsilon^{(4)}_{i+\frac{1}{2},j}(Q_{i+2,j} \quad 3Q_{i+1,j}+3Q_{i,j} \quad Q_{i \quad 1,j})\right], \tag{13}$$

where A is the Jacobian matrix of the convective flux in the i direction. There are also similar expressions for the j direction. Let Λ be the diagonal matrix with the eigenvalues of A along its diagonal:

$$\Lambda = \mathrm{diag}(\lambda_1, \lambda_2, \lambda_3, \lambda_3), \tag{14}$$

where:

$$\lambda_1 = q + c\sqrt{a_1^2 + a_2^2}, \qquad \lambda_2 = q \quad c\sqrt{a_1^2 + a_2^2},$$
$$\lambda_3 = q, \tag{15}$$

a_1, a_2 and q are defined like Equation 12. Then:

$$|A| = |\lambda_3|I + \left(\frac{|\lambda_1| + |\lambda_2|}{2} \quad |\lambda_3|\right)$$
$$\times \left[\frac{\gamma \quad 1}{c^2}E_1 + \frac{1}{a_1^2 + a_2^2}E_2\right]$$
$$+ \frac{|\lambda_1| \quad |\lambda_2|}{2}\left(\frac{1}{\sqrt{a_1^2 + a_2^2}c}\right) \times [E_3 + (\gamma \quad 1)E_4], \tag{16}$$

where E_1, E_2, E_3 and E_4 are the 4×4 matrices, the arrays of which are functions of the velocity components, local kinetic energy, total enthalpy, a_1, a_2 and q. For more details of matrix $|A|$ and factors $\varepsilon^{(2)}$ and $\varepsilon^{(4)}$, see [21]. The disadvantage of MADS models is that, in general, they increase the operation count for processing mesh points by a factor of about 1.4 times greater than that required by SCDS models.

Convective Upstream Split Pressure (CUSP)

This dissipation scheme was presented by Tatsumi et al. [22]. It is a flux splitting and limiting technique, which yields a one-point stationary shock capturing. For simplicity, consider the one-dimensional form of Equation 1, which can be expressed as:

$$Q_t + f_x = 0. \tag{17}$$

This scheme is an intermediate type of scheme, which can be formulated by defining the first order diffusive flux as a combination of differences of the state and flux vectors:

$$d_{i+\frac{1}{2}} = \frac{1}{2}\alpha^*_{i+\frac{1}{2}}c(Q_{i+1} \quad Q_i) + \frac{1}{2}\beta_{i+\frac{1}{2}}(f_{i+1} \quad f_i). \tag{18}$$

Decomposition of the flux vector, f, yields:

$$f = uQ + f_p, \tag{19}$$

where:

$$f_p = \begin{pmatrix} 0 \\ P \\ uP \end{pmatrix}. \tag{20}$$

Then:

$$f_{i+1} \quad f_i = \overline{u}(Q_{i+1} \quad Q_i) + \overline{Q}(u_{i+1} \quad u_i) + f_{p_{i+1}} \quad f_{p_i}, \tag{21}$$

where $\overline{u}$ and $\overline{Q}$ are the arithmetic averages of velocity and flow rate, respectively. If the convective terms are separated by splitting the flux, according to Equations 19 to 21, it will be called E-CUSP. For further information about the total effective coefficient of convective diffusion ($\alpha^* c$) and β, see [22].

ANALYSIS OF CONFINEMENT PARAMETER

As pointed out in the introduction, a dimensional analysis of the confinement term shows that the confinement parameter has the dimension of velocity. This means that, for a given grid and configuration, a proper choice of this parameter should be dependent on the local stream conditions of the flow field and the mesh cell size.

Reviewing all dissipation schemes, one can find that all of them use Jacobian matrices or the corresponding eigenvalues as the scaling velocity. On the other hand, the vorticity confinement term is in the form of anti-diffusion. As a result, here, three confinement parameters are introduced as the scaling velocity, which have been extracted from these dissipation schemes.

SCalar Confinement Parameter (SCCP)

Here, the confinement parameter is derived from the spectral radii of the flux Jacobian matrix. First, the vorticity confinement term is defined as:

$$S = \begin{bmatrix} 0 \\ \rho E_{cx} \omega_z \phi_{ys} \\ \rho E_{cy} \omega_z \phi_{xs} \\ \rho[u E_{cx}(\ \ \omega_z \phi_{ys}) + \nu E_{cy}(\omega_z \phi_{xs})] \end{bmatrix}, \tag{22}$$

where E_{cx} and E_{cy} are the functions of the spectral radii of the flux Jacobian matrix. E_{cx} is defined as:

$$E_{cx} = \varepsilon \frac{|\lambda|_{i,j}}{\sqrt{a_1^2 + a_2^2}}, \tag{23}$$

where $|\lambda|_{i,j}$, a_1 and a_2 were defined in Equations 11 and 12. Substituting for a_1 and a_2 from the following to Equations 23 and 11, an equation like Equation 23 for the y direction (E_{cy}) will be found:

$$a_1 = J^{\ -1}\eta_x, \qquad a_2 = J^{\ -1}\eta_y. \tag{24}$$

One can see that E_{cx} and E_{cy} have the dimension of velocity. Thus, the confinement parameter implicitly contains the grid sizes and fluid properties as a scaling factor.

MAtrix Confinement Parameter (MACP)

Here, the confinement parameter is derived from the flux Jacobian matrix. The vorticity confinement term is defined as:

$$S = S_x + S_y, \tag{25}$$

where:

$$S_x = |A'| \begin{pmatrix} 0 \\ \varepsilon\rho(\hat{n} \times \vec{\omega}).\hat{i} \\ 0 \\ \varepsilon\rho(\hat{n} \times \vec{\omega}).u\hat{i} \end{pmatrix},$$

$$S_y = |B'| \begin{pmatrix} 0 \\ 0 \\ \varepsilon\rho(\hat{n} \times \vec{\omega}).\hat{j} \\ \varepsilon\rho(\hat{n} \times \vec{\omega}).v\hat{j} \end{pmatrix}, \tag{26}$$

and $|A'|$ and $|B'|$ are defined as:

$$|A'| = \frac{|A|}{\sqrt{a_1^2 + a_2^2}}, \qquad |B'| = \frac{|B|}{\sqrt{a_1^2 + a_2^2}}, \tag{27}$$

where a_1 and a_2 are defined, based on Equation 12 for $|A'|$ and Equation 24 for $|B'|$.

Convective Upstream Split Pressure Confinement Parameter (CUCP)

An important property of the CUSP scheme can be illustrated by introducing a Roe linearization and rewriting the diffusive flux of Equation 18 as:

$$d_{i+\frac{1}{2}} = \frac{1}{2}\left(\alpha^* cI + \beta A_{i+\frac{1}{2}}\right)(Q_{i+1} \quad Q_i), \tag{28}$$

where $A_{i+\frac{1}{2}}$ is an estimate of the Jacobian matrix, $\frac{\partial f}{\partial Q}$, obtained by Roe linearization of Equation 16, with the condition that the following equation:

$$f_{i+1} \quad f_i = A_{i+\frac{1}{2}}(Q_{i+1} \quad Q_i),$$

is exactly satisfied. Therefore, by introducing $|\Theta|$ and $|\Xi|$ as follows:

$$|\Theta| = \frac{1}{2}\left(\alpha^* cI + \beta|A|\right), \qquad |\Xi| = \frac{1}{2}\left(\alpha^* cI + \beta|B|\right), \tag{29}$$

the vorticity confinement terms of Equation 25 are defined as:

$$S_x = |\Theta'| \begin{pmatrix} 0 \\ \varepsilon\rho(\hat{n} \times \vec{\omega}).\hat{i} \\ 0 \\ \varepsilon\rho(\hat{n} \times \vec{\omega}).u\hat{i} \end{pmatrix},$$

$$S_y = |\Xi'| \begin{pmatrix} 0 \\ 0 \\ \varepsilon\rho(\hat{n} \times \vec{\omega}).\hat{j} \\ \varepsilon\rho(\hat{n} \times \vec{\omega}).v\hat{j} \end{pmatrix}, \tag{30}$$

where $|\Theta'|$ and $|\Xi'|$ are defined as:

$$|\Theta'| = \frac{|\Theta|}{\sqrt{a_1^2 + a_2^2}}, \qquad |\Xi'| = \frac{|\Xi|}{\sqrt{a_1^2 + a_2^2}}. \tag{31}$$

In all of the above equations, ε (tuning constant) is a non-dimensional constant and must be tuned for each test case.

RESULTS AND DISCUSSION

Three test cases are considered here to demonstrate the application of the new variable confinement parameters (SCCP, MACP and CUCP). The calculations were performed with the three dissipation schemes, once with compressible vorticity confinement and once without.

Vortex Moving in a Uniform Flow

As a basic test of the ability of the new confinement parameters, two cases of convecting concentrated vortex, a single vortex moving in a uniform flow along a coordinate direction and the same vortex convecting in a uniform flow at an angle to x axis, were tested.

Vortex Moving in a Uniform Flow Along a Coordinate Direction

A vortex moving with a uniform stream is tested initially. The computational boundary is a square domain of 1×1 m^2. Periodic boundary conditions are set at all sides of the domain. The computed vortex, then, passes through the grid and reappears on the other side. The initial condition of the vortex is set up, according to Povitsky and Ofengeim [23]. The tangential velocity distribution is prescribed between an outer radius, $r = R_o$, and a core radius, $r = R_c$. For radius greater than R_o, the tangential velocity of the vortex is set to zero. The tangential velocity of the vortex can be expressed, as follows:

$$u_\theta(r) = \begin{cases} U_c \frac{r}{R_c}, & r < R_c \\ Ar + \frac{B}{r}, & R_c \leq r \leq R_o \end{cases}$$

where:

$$A = \frac{U_c R_c}{R_o^2 \quad R_c^2}, \qquad B = \frac{U_c R_c R_o^2}{R_o^2 \quad R_c^2},$$

that results in $u_\theta(0) = 0$, $u_\theta(R_c) = U_c$ and $u_\theta(R_o) = 0$. The velocity, u_θ, at R_c reaches U_c, which is the maximum velocity magnitude of the whole domain and is a parameter set before calculation.

The initial vortex is imposed on a uniform free stream and the center of the vortex is located in $(0, 0)$ of the Cartesian coordinates. The calculation were performed with $R_c = 0.05$ m, $R_o = 10\ R_c$, $a_\infty = 347.2\ \frac{\text{m}}{\text{sec}}$, $M_\infty = 0.5$ and $U_c = U_\infty$. In order to investigate the effect of a non-uniform grid on the solution, the grid was stretched non-uniformly in two dimensions, similar to the grid described in [8]; the resulting mesh for 100×100 grid points is shown in Figure 1.

The calculation was performed with three dissipation schemes, once with vorticity confinement and once without. The analytic solution for a compressible vortex moving with a uniform freestream is discussed

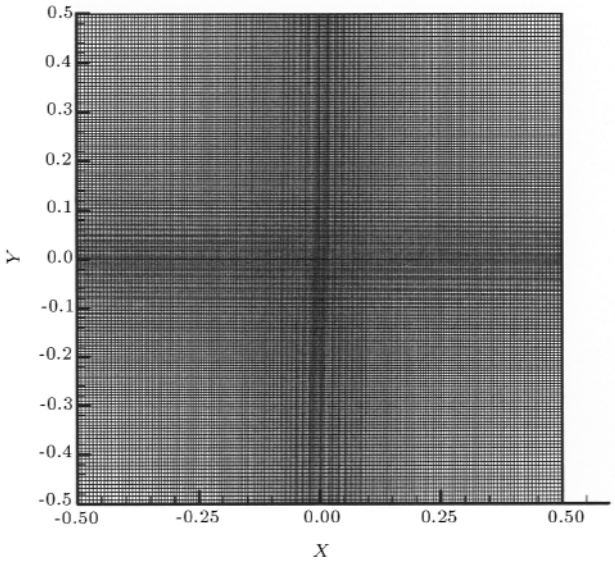

Figure 1. Sample grid for calculation of a moving vortex in a uniform compressible flow.

in [4]. The solution contains the well-known result that the quantity, $\frac{\omega}{\rho}$, of a vortex will be conserved as it convects in a compressible, inviscid, adiabatic fluid.

Contours of the initial $\frac{\omega}{\rho}$ distribution are presented in Figure 2. Figures 3 to 5 present the contours of the quantity, $\frac{\omega}{\rho}$, of the flow without confinement, after the vortex has passed through the grid ten cycles and, approximately, backed to the center of the computational domain. The calculations are for SCDS, MADS and CUSP. The degree of dissipation can be seen clearly in these figures.

Figures 6 to 8 present the results of the same calculations but with the vorticity confinement using SCCP, MACP and CUCP. These figures are, essentially, identical to each other; no dissipation is seen

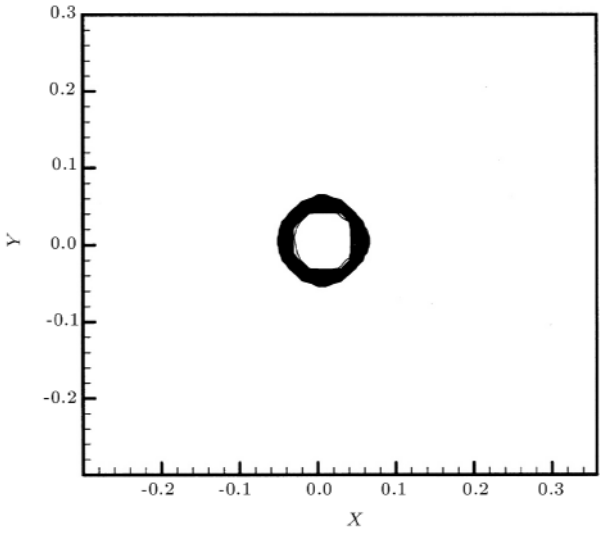

Figure 2. Contours of the quantity $\frac{\omega}{\rho}$ of the vortex at the beginning.

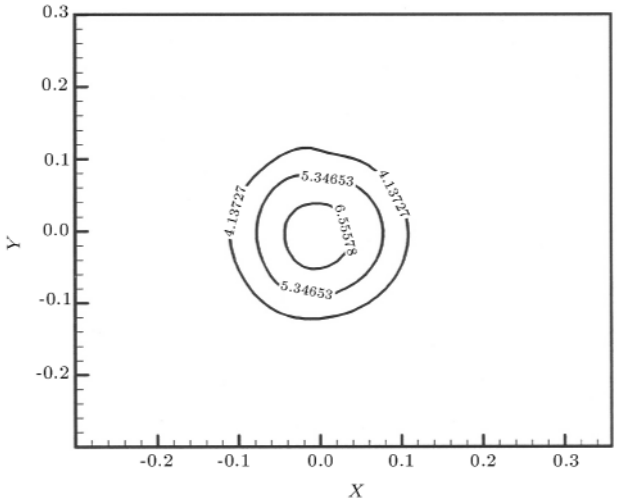

Figure 3. Contours of the quantity $\frac{\omega}{\rho}$ of the vortex after ten cycle - no CVC (SCDS).

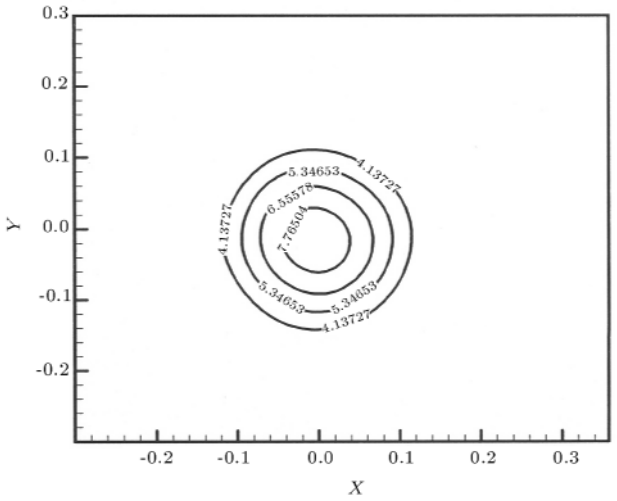

Figure 4. Contours of the quantity $\frac{\omega}{\rho}$ of the vortex after ten cycle - no CVC (MADS).

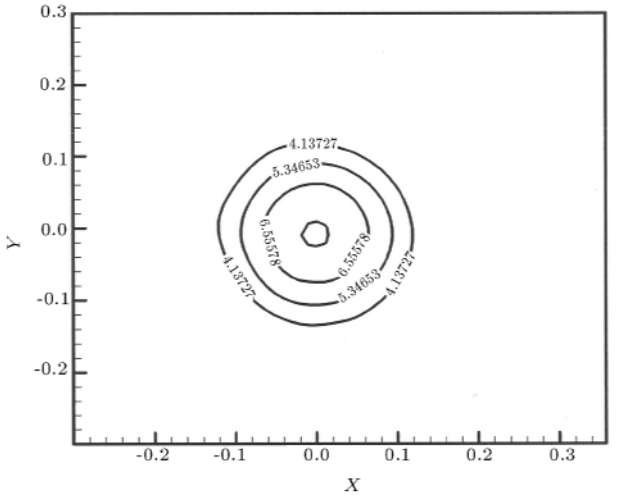

Figure 5. Contours of the quantity $\frac{\omega}{\rho}$ of the vortex after ten cycle - no CVC (CUSP).

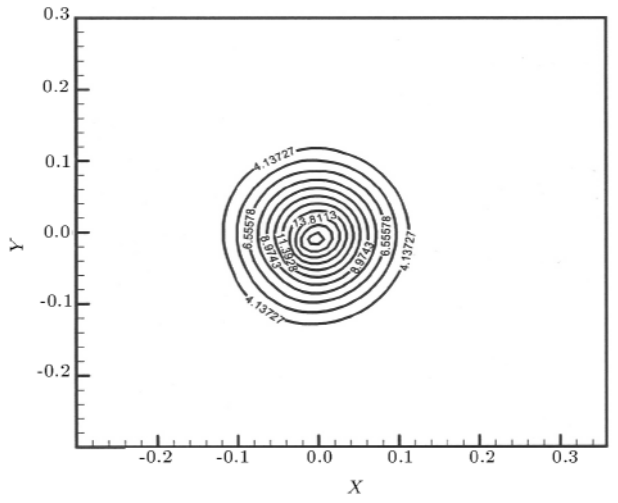

Figure 6. Contours of the quantity $\frac{\omega}{\rho}$ of the vortex after ten cycle - CVC (SCCP).

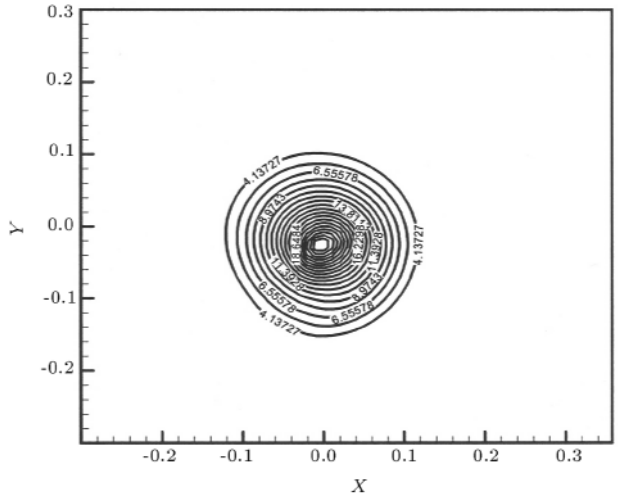

Figure 7. Contours of the quantity $\frac{\omega}{\rho}$ of the vortex after ten cycle - CVC (MACP).

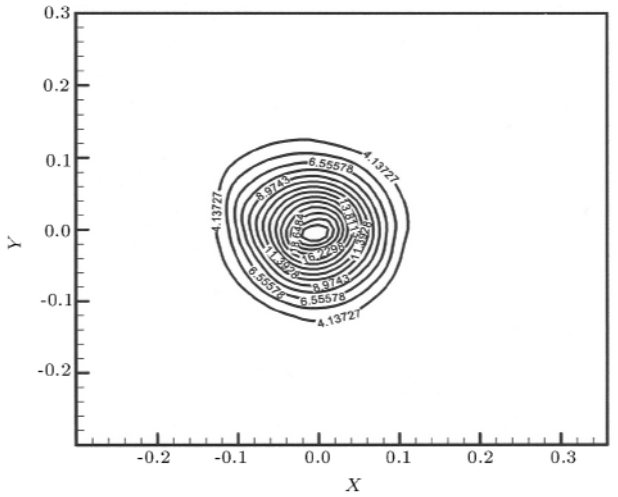

Figure 8. Contours of the quantity $\frac{\omega}{\rho}$ of the vortex after ten cycle - CVC (CUCP).

in these figures. The magnitude of ε was set to 0.0025, 0.005 and 0.025 for the three confinement methods of SCCP, MACP and CUCP, respectively. It is observed that the value of ε for CUCP is the maximum and for SCCP is the minimum. But, it is still time-consuming to find ε as in the original method (constant confinement parameter). The properties of the introduced schemes are such that the confinement parameters are functions of fluid properties and mesh size at each location and ε is a non-dimensional parameter. It must be mentioned that 30 contour levels were used to plot all the Figures 3 to 8.

The profile of the quantity, $\frac{\omega}{\rho}$, along a diameter of the moving vortex is presented in Figure 9. The solutions without confinement seem to be the result of a very diffusive flow with a viscosity even bigger than the real fluid viscosity. This quantity vanishes as the vortex moves along with the uniform free stream, because there is no "force" to balance the numerical dissipation. An inviscid flow is, however, being solved and no diffusive effects are expected. This means that the vorticity should not have spread. Also, the diffusive characteristics of the numerical solutions are seen in Figures 3 to 5. On the other hand, the solution with confinement does not show the dissipative behavior of the solution without confinement, even though the vortex moved for ten cycles and backed to, about the original place. It is, approximately, close to the analytical solution. From this fact, one may conclude that the vorticity confinement nearly cancels most of the numerical dissipation errors, to conserve the quantity, $\frac{\omega}{\rho}$, of the vortex.

Finally, the calculations showed that, if a constant confinement parameter (Hu et al. confinement, Equation 2) was used, E_c would have a value of 0.0025 (for all dissipation schemes).

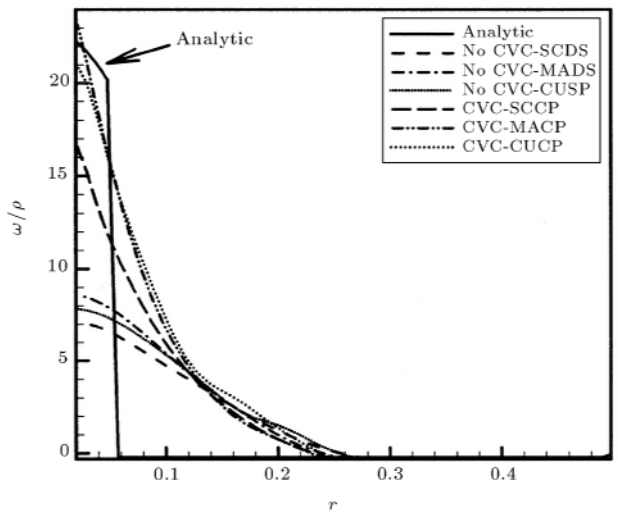

Figure 9. Profile of the quantity $\frac{\omega}{\rho}$ across the diameter of the vortex.

Vortex Moving in a Uniform Flow at an Angle to x Axis

In this case, the vortex mentioned above is imposed on a uniform flow, moving at an angle of 35 degrees with the x axis. The vortex center is located in (0, 0) of the Cartesian coordinates at the beginning. The vortex and free stream conditions are the same as those of the vortex in part A. A 200×200 uniform mesh and 1300 time steps were used for this calculation. Two solutions are presented, one without confinement (using the CUSP dissipation scheme) and one with confinement (the CUCP scheme).

Figure 10 shows the contours of the quantity, $\frac{\omega}{\rho}$, with 27 different levels. The contours are plotted at each 100 time-step intervals, making a total of 13 plots. For the whole simulation, the vortex has traveled 168 and 117 cells in the x and y directions, respectively. It can be seen that numerical diffusion results in an extensive spreading of the vortex as time increases.

Results with the confinement scheme (CUCP, $\varepsilon = 0.025$), at the same time steps, are presented in Figure 11. The same contour levels as of Figure 10 were used for this figure. Compared to Figure 10, no extensive spreading of the vortex is seen in Figure 11. The vortex center has moved 167 cells in the x direction and 116 cells in the y direction, after application of confinement. Similar results can be obtained using two other schemes (SCCP, MACP), which are not shown here.

Supersonic Base Flow

In practical problems, the Reynolds numbers are very high. Thus, the values of viscous terms in Navier-Stokes equations are much smaller than those of the convection terms. It was attempted to simulate the

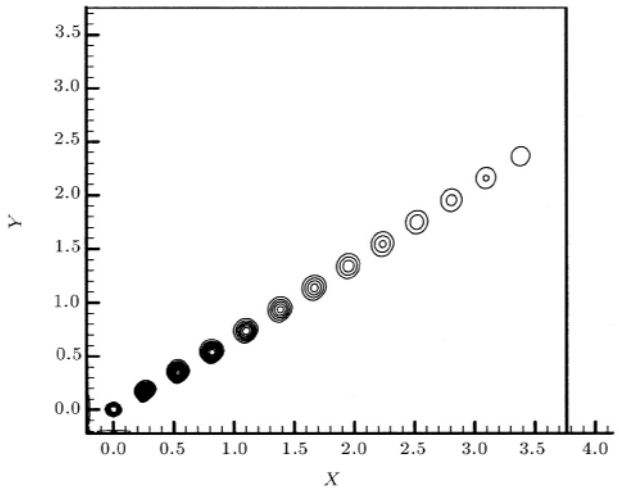

Figure 10. Contours of the quantity $\frac{\omega}{\rho}$ of the vortex moving in a uniform flow at an angle of 35 degree to the x axis after 1300 time steps - no CVC (CUSP).

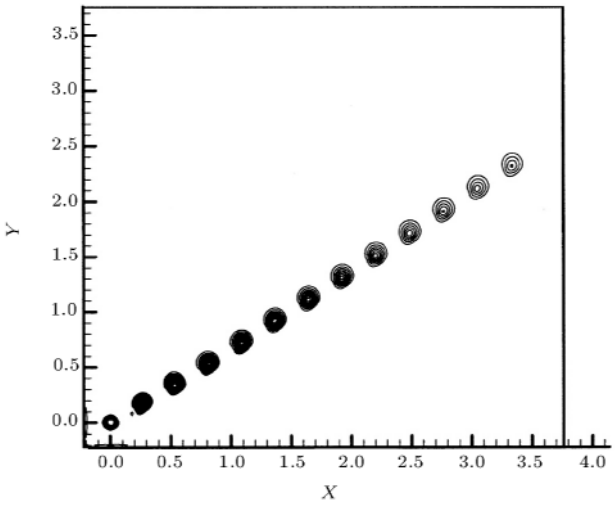

Figure 11. Contours of the quantity $\frac{\omega}{\rho}$ of the vortex moving in a uniform flow at an angle of 35 degree to the x axis after 1300 time steps - CVC (CUCP).

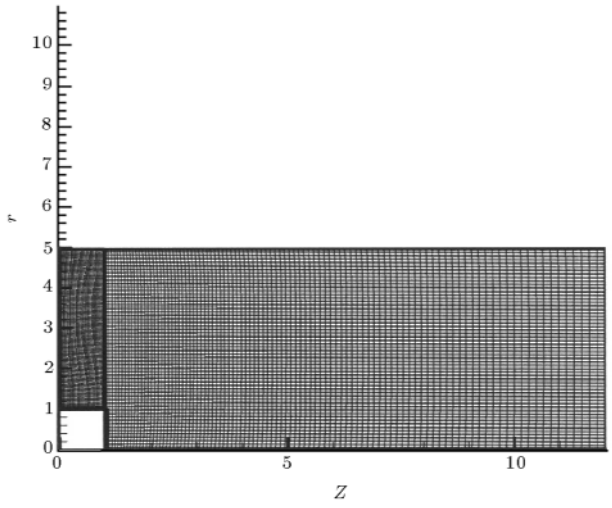

Figure 12. Grid over the base (r z plane).

problems mentioned above, using Euler equations. However, the boundary layer near the wall could not be ignored, because of its importance in vortex-dominant flows. Therefore, no-slip conditions were used in all the calculations to enforce the viscous flow boundary conditions on the wall.

Hu [4] showed that the solution of Euler equations for a flow over a flat plate with Mach number of M = 0.1 and Reynolds number of Re = 2×10^5, results in a velocity profile similar to that of a laminar flow, if a no-slip condition is used. The velocity profile, however, becomes similar to that of a turbulent flow (especially close to the wall), if the compressible vorticity confinement is applied. As a result, Hu [4] stated that Euler equations with the use of CVC may be used to model turbulent flow in the near wall region. Therefore, using this approximate profile for modeling the separated vortex from the base, which is strongly dependent on the upstream-attached-flow before the trailing edge, is reasonable.

The second case is a supersonic axisymmetric base flow. The near wake of a circular cylinder, aligned with a uniform Mach 2.45, has been experimentally investigated by Herrin and Dutton [24].

The non-uniform computational grid of 200×100 is shown in Figure 12 (r z plane). No penetration condition was enforced at the solid walls, free-stream conditions in the upstream of the base and the symmetry condition at the symmetry plane.

The streamlines and pressure contours at the base region are presented in Figures 13 and 14, which show the primary vortex, expansion waves and recompression region. The pressure reaches a minimum in the core of the vortex. Figure 13 shows the results without applying a vorticity confinement, using the CUSP dissipation scheme. Experimental results [24]

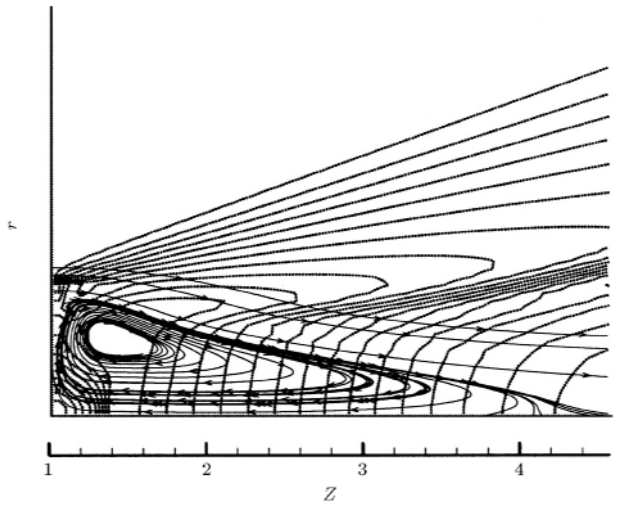

Figure 13. Streamlines and pressure contours at the base region - no CVC (CUSP).

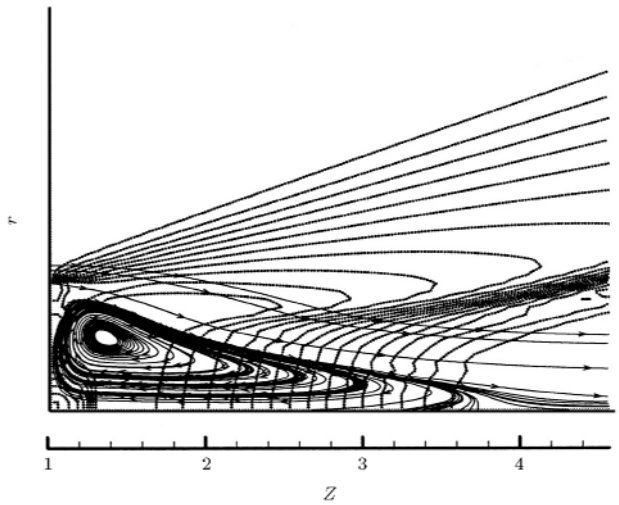

Figure 14. Streamlines and pressure contours at the base region - CVC (CUCP).

show that the reattachment point is about 2.65 times the radius of the base. Without applying the vorticity confinement, the reattachment point is greater than 3. The length of the reattachment point is about $x = 3.08$, 3.32 and 3.1 for SCDS, MADS and CUSP schemes, respectively. Therefore, the dissipation of the vortex flow is clearly seen in Figure 13. Figure 14 shows the same computation results, but, with the confinement in effect (CUCP). The streamlines indicate practically no degradation of the vortex. Values of ε are 0.03, 0.05 and 0.07 for SCCP, MACP and CUCP schemes, respectively. It is seen that the CUCP parameter has the highest value and the SCCP parameter has the least.

The same calculation was done with the constant confinement parameter (Hu et al. scheme, Equation 2). It was obtained that E_c would have a value of 0.03. These figures only show the qualitative information, such as shock, vortex, and vortex/shock interactions. The pressure coefficient profile on the surface of the base and its comparison with experimental results will give the quantitative information.

Pressure coefficient distribution at the base region is shown in Figure 15. The results are over-estimated near the centerline ($r = 0$) and are under-estimated near the base top ($r = 1$), for no confinement calculations. This trend is also seen for SCCP and CUCP. However, SCCP and CUCP results are closer to the experimental results of Herrin and Dutton [24], near the centerline. The main discrepancy occurs near the base top portion. Good results in this portion are obtained using the SCDS dissipation scheme, without CVC, SCCP and CUCP schemes. Unlike the good performance of the CUCP scheme, in general, it increases the operation count for processing mesh points greater than that required by the SCCP scheme. The same increase is seen using the MACP scheme. The reason is related to the matrix product used in these schemes.

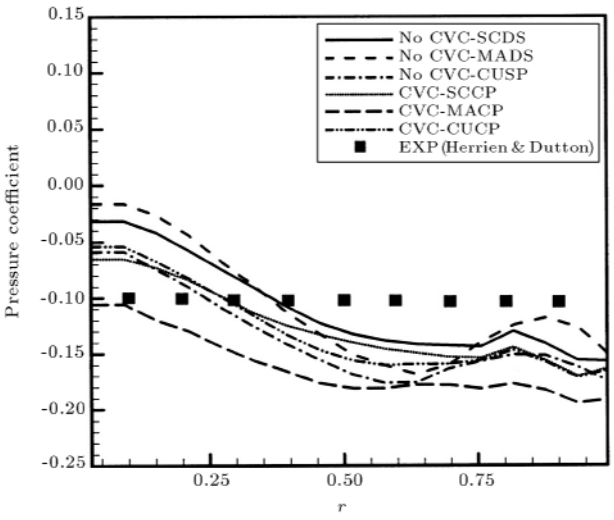

Figure 15. Pressure coefficient at the base region.

Supersonic Shear Layer

An inviscid supersonic shear layer flow is formed by two parallel streams, one at Mach number $M = 2.4$ and the other at $M = 2.9$. The two streams flow at an angle of 30 degrees relative to the horizontal grid line. The computational grid is a 100×100 uniform Cartesian grid. The three dissipation schemes were used with and without confinement.

Figures 16 and 17 show the Mach number contours of the flow solution after 1000 time steps. Figure 16 presents the result of the calculation without the vorticity confinement. The dissipation scheme used for this calculation is scalar. The dissipation of the shear

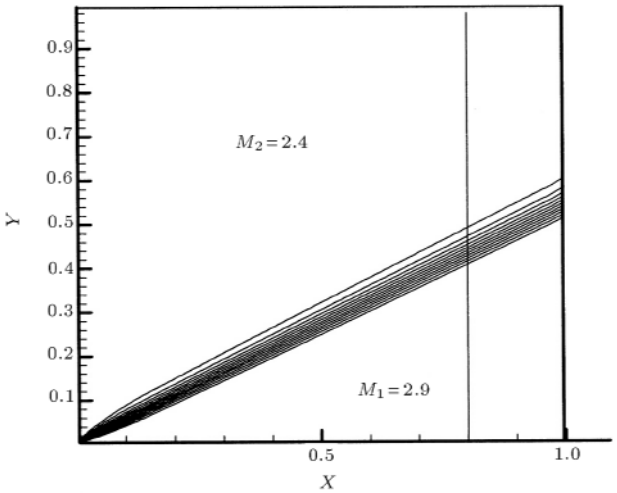

Figure 16. The mach contours of inviscid supersonic shear layer - no CVC (SCDS).

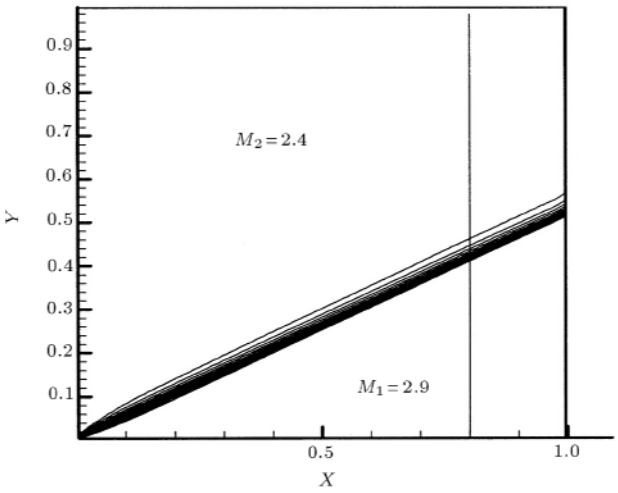

Figure 17. The mach contours of inviscid supersonic shear layer - CVC (SCCP).

layer is clear from the figure. The same results are observed for the other dissipation schemes. Figure 17 shows the same computational result, but, using the SCCP method. No degradation of the shear layer is seen in this figure with application of the new vorticity confinement. The same results can be obtained with the other vorticity confinements, but they are not shown here.

Figure 18 presents the Mach number profile computed without confinement (using SCDS and CUSP) and with confinement (using SCCP, MACP and CUCP) along a cutting line parallel to the vertical axis ($x = 0.8$). From the Mach profiles, it is seen that, without confinement, the solution is significantly degraded. Applying CUCP will sharpen the discontinuity better than the other schemes. However, SCDS and MADS (not shown here) eventually develop a little overshoot after the shear layer in the profile. The ε values of 0.01, 0.015 and 0.025 were used for the SCCP, MACP and CUCP schemes, respectively. If a constant confinement parameter (Hu et al. scheme [8]) was used, E_c would have a value of 0.01.

Comparing the parameter, ε, for the new confinements with the constant confinement presented by Hu et al. [8], for the above three cases, shows that, when variable confinement parameters (SCCP, MACP and CUCP) are used, the parameter ε is equal (for SCCP) or larger (for MACP and CUCP) than the equivalent value of the constant confinement (E_c). That is because the new confinement parameters implicitly contain the effects of grid sizes and flowfield properties as the scaling factors. On the other hand, based on the authors experiences, the value of ε ranges at a smaller limit than the constant confinement parameter for three cases, especially for the CUCP scheme.

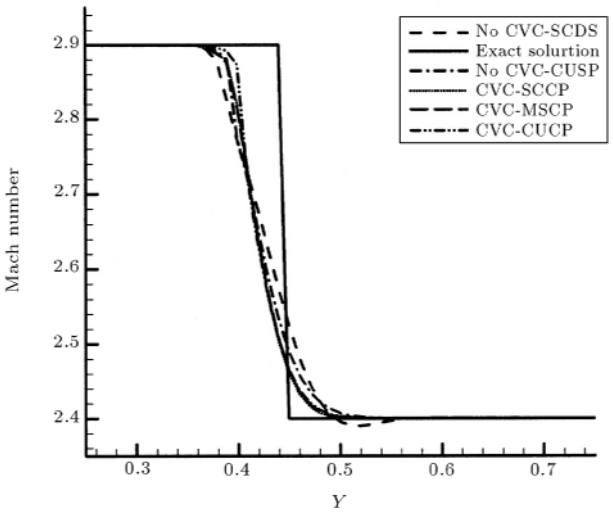

Figure 18. The mach profile along a cut line that parallels to the vertical axis.

SUMMARY AND CONCLUSION

In this paper, the compressible vorticity confinement of Hu et al. [8] has been successfully developed. Three variable confinement parameters, which have velocity dimension, were defined, based on three artificial dissipation schemes. The resulting confinement parameters are functions of the spectral radii of the Jacobian matrices and the Jacobian matrices themselves. So, the confinement parameter implicitly contains the grid size and other local fluid properties.

Preliminary results for the subsonic moving vortices showed that the new confinement parameters allow the capture of vortical layers that effectively do not decay in time, similar to the confinement of Hu et al. [8]. Calculation of the supersonic base flow and supersonic shear layer showed good agreement with experimental and analytical data for the variable CUSP confinement parameter (CUCP). The matrix and CUSP confinement parameters are computationally expensive, while the scalar confinement parameter is economical. However, the same problem for tuning the confinement parameter still exists.

Finally, when variable confinement parameters are used, the tuning constant is equal to or larger than, the equivalent value of the constant confinement (Hu et al. [8]). This means that this value ranges within a smaller limit than that of the constant confinement parameter, especially for the CUCP scheme.

ACKNOWLEDGMENT

The authors would like to thank Dr. M.P. Fard of the Ferdowsi University of Mashhad for reviewing the paper.

REFERENCES

1. Benoit, C. "Numerical simulation of 2D blade vortex interaction using moving overset grids", in *25th European Rotorcraft Forum*, Roma, Italy (Sept. 1999).
2. Ochi, A., Aoyama, T., Saito, S., Shima, E. and Yamakawa, E. "BVI noise predictions by moving overlapped grid method", in *AHS 55th Annual Forum*, Montréal, Québec, Canada (May 1999).
3. Visbal, M.R. and Gaitonde, D.V. "High-order accurate methods for unsteady vortical flows on curvilinear meshes", in *AIAA 36th Aerospace Sciences, Meeting and Exhibit*, Reno, NV, USA (January 1998).
4. Hu, G. "The development and applications of a numerical method for compressible vorticity confinement in vortex-dominant flows", *Ph.D. Dissertation, Dept. of Aerospace and Ocean Engineering*, Virginia Polytechnic Inst. and State Univ., Blacksburg, VA, USA (June 2001).
5. Steinhoff, J., Wang, C., Underhill, D., Mersch, T. and Wenren, Y. "Computational vorticity confinement: A

non-diffusive Eulerian method for vortex-dominated flows", *UTSI*, preprint (1992).

6. Steinhoff, J. and Underhill, D. "Modification of the Euler equations for vorticity confinement application to the computation of interacting vortex rings", *Physics of Fluids*, **6**, pp 2738-2744 (1994).
7. Steinhoff, J. "Vorticity confinement: A new technique for computing vortex dominated flows", *Frontiers of Computational Fluid Dynamics*, D.A. Caughey and M.M. Hafez, Eds., John Wiley & Sons, pp 235-264 (1994).
8. Hu, G., Grossman, B. and Steinhoff, J. "Numerical method for vorticity confinement in compressible flow", *AIAA Journal*, **40**(10), pp 1945-1953 (Oct. 2002).
9. Wenren, Y., Fan, M., Dietz, W., Hu, G., Braun, C., Steinhoff, J. and Grossman, B. "Efficient Eulerian computation of realistic rotorcraft flows using vorticity confinement - a survey of recent results", in *39th AIAA Aerospace Sciences Meeting and Exhibit*, Reno, NV, USA (Jan. 2001).
10. Wenren, Y., Steinhoff, J., Wang, L., Fan, M. and Xiao, M. "Application of vorticity confinement to the prediction of the flow over complex bodies", in *AIAA Fluids 2000*, Denver, CO (June 2000).
11. Wenren, Y., Fan, M., Wang, L., Xiao, M. and Steinhoff, J. "Application of vorticity confinement to prediction of the flow over complex bodies", *AIAA Journal*, **41**(5), pp 809-816 (May 2003).
12. Pevchin, S., Grossman, B. and Steinhoff, J. "Capture of contact discontinuities and shock waves using a discontinuity confinement procedure", *AIAA Paper 97-0874* (Jan. 1997).
13. Yee, K. and Lee, D.H. "Euler calculation for a hovering coaxial rotor flow field with new boundary condition", *Proceeding of the 24th European Rotorcraft Forum*, Marseilles, France, pp AE-1-AE-10 (1998).
14. Murayama, M., Nakahashi, K. and Obayashi, S. "Numerical simulation of vortical flows using vorticity confinement coupled with unstructured grid", in *39th AIAA Aerospace Sciences Meeting and Exhibit*, Reno, NV, USA (Jan. 2001).
15. Fedkiw, R., Stam, J. and Jensen, H.W. "Visual simulation of smoke", in *Proc. SIGGRAPH 2001*, pp 15-22, Los Angeles, CA, USA (2001).
16. Lohner, R. and Yang, C. "Tracking vortices over large distances using vorticity confinement", *ECCOMAS, CFD 2001*, Swansea, Wales, UK (Sept. 2001).
17. Costes, M. and Kowani, G. "An automatic anti-diffusion method for vortical flows based on vorticity confinement", *Aerospace Science and Technology*, **7**, pp 11-21 (2003).
18. Pulliam, T.H. and Chausse, D.S. "A diagonal form of an implicit approximation-factorization algorithm", *J. Comput. Phys.*, **39**, pp 347-363 (1981).
19. Jameson, A., Schmidt, W. and Turkel, E. "Numerical simulation of the Euler equations by finite volume methods using Runge-Kutta time stepping schemes", *AIAA Paper 81-1259* (1981).
20. Jameson, A. "The present status, challenges and future developments in computational fluid dynamics", *Conference, the University of Sydney*, Australia (1995).
21. Swanson, R.C. and Turkel, E. "On central-difference and upwind schemes", *J. Comput. Phys.*, **101**, pp 292-306 (1992).
22. Tatsumi, S., Martinelli, L. and Jameson, A. "A new high resolution scheme for compressible viscous flows with shocks", *AIAA 95-0466, 33rd Aerospace Science Meeting Exhibit*, January 9-12, Reno, USA (1995).
23. Povitsky, A. and Ofengeim, D. "Numerical study of interaction of a vortical density inhomogeneity with shock and expansion waves", *NASA/CR-206918*, ICASE Report No. 98-10 (1998).
24. Herrin, J.L. and Dutton, J.C. "Supersonic base flow experiments in the near wake of a cylindrical afterbody", *AIAA Journal*, **32**(1), pp 77-83 (Jan. 1994).